Johan Forsberg, Ulf Larsson and Åke Wernersson

# Mobile Robot Navigation using the Range-Weighted Hough Transform

Using a range-measuring laser, the range-weighted Hough transform and the extended Kalman filter, the authors demonstrate accurate and robust navigation of a mobile robot through cluttered rooms.


## ABSTRACT

Accurate navigation of a mobile robot in cluttered rooms using a range-measuring laser as a sensor has been achieved. To extract the directions and distances to the walls of the room the range-weighted Hough transform is used. The following experimental results are emphasized:

- The robot extracts the walls of the surrounding room from the range measurements. The distances between parallel walls are estimated with a standard deviation smaller than 1 cm.
- It is possible to navigate the robot along any preselected trajectory in the room. One special case is navigation through an open door detected by the laser. The accuracy of the passage is 1 cm at a speed of 0.5 m/s. The trajectory is perpendicular to the wall within 0.5 degrees in angle.
- When navigating through corridors, the accuracy is better than 1 cm at 0.8 m/s - the maximum speed of the robot.

Odometric data and laser measurements are combined using the extended Kalman filter. The size of the cluttered rectangular room and the position and orientation (pose) of the robot are estimated during motion. The extraction and the resulting navigation are very *robust* against both spurious measurements in the laser measurements and disturbing objects.


## INTRODUCTION

A method for navigating a mobile robot in cluttered rooms and corridors is introduced and tested using the robot in Fig. 1. The localization of the robot is performed relative to the walls of an indoor environment. The area around the robot is measured using an on-board scanning time-of-flight laser. The observations of the walls are extracted using the range-weighted Hough transform (RWHT) and the position of the robot is continuously updated using an extended Kalman filter (EKF). The experimental tests presented concern navigation in one room at a time. This is useful as a proof of concepts, and makes the result clearer and easier to understand. A complete map-building and navigation system along these lines is under development with preliminary results given in [14].

*Johan Forsberg, Ulf Larsson and Åke Wernersson: Robotics & Automation, Luleå University of Technology, S-971 87 Luleå, Sweden. E-mail: robotics@sm.loth.se.*

### Different Sensor Systems and Related Work

Robot navigation is generally based on a combination of internal sensors (like odometers and rate gyros) for dead reckoning and external sensors (like time-of-flight lasers) for finding objects in the surroundings of the robot and for locating external position references. Robot navigation is a wide research area with numerous contributions including books like [6] and [15]. Navigation can use external references and landmarks occurring naturally in the environment like walls and tree trunks. Landmarks can also be artificial as in navigation using radio beacons (including GPS) and, for indoor navigation, retroreflective tape as in [11].

To put this contribution in its proper context some of the sensing principles used for mobile robot navigation are outlined in Table 1. The first column is for the scanning time-of-flight laser used in this paper. The second column is for a typical ultrasonic system. The last column is for a navigation system where a rotating laser measures angles to several identical beacons consisting of stripes of retroreflective tape.

Actual navigation experiments using ultrasonics have been carried out in several laboratories (see [4]

**Table 1 Typical Sensors for Mobile Robot Navigation.**

| | Time-of-flight laser | Ultrasonics | Laser beam and reflectors |
|---|---|---|---|
| Beam width | 0.04+ 0.002 R m. | 0.03+ 0.2R m. | 0.001+ 0.001 R m |
| Sampling | 0.25 ms | 20-100 ms | (0.1 ms) |
| Side lobes | None | 13 dB | None |
| Spurious measurements | Few | Many | Very few |
| Dropouts | Many | Few | Not Critical |
| Useful range | 0.5-30m | 0.1-5m | 0.2-100m |
| Range resolution | $\sigma$ = 2cm. | $\sigma$ = 1cm. | — |

and [15]). Ultrasonics has the drawback that the angular resolution is poor and spurioses are common, [15]. This makes direct use of ultrasonics difficult. To improve resolution an uncertainty grid and a Bayesian type of filtering are used in [7]. In [16] ultrasonics is used to build a feature-based map. Modelling and simulation efforts as in [10] are important as well as the basic physics [21].

An alternative technology is scanning range-measuring time-of-flight lasers. The range resolution is about the same as that for ultrasonics, but the angular resolution is much better and there are less spurioses. The combined advantages result in the time-of-flight laser generally giving a high-resolution two-dimensional scan of the robot's environment in a fraction of a second. In [5] it is described how a scanning range-measuring laser can be used to correct the position errors introduced during dead reckoning. A direct matching of range data to an *a priori* map is used to find the corrections. Mutual dependencies are modelled in [19] and tested experimentally. Map building and path planning among polygonal objects are the subject of [9]. Simulations are made with a perfect dead reckoning assumption.

Vision and stereovision in combination with extended Kalman filters have been used in [3]. In [2] a set-based algorithm is used to achieve very low computation times. The third column in Table 1 is a very special type of 'vision'-based navigation [11], [22]. Stripes of retroreflective tape are used as landmarks making the image processing both simple and robust. This navigation system is in fact in industrial use for AGV navigation. The repeatability is better than 0.5 cm at full speed.

One contribution in this paper is the extraction of walls using the Hough transform (HT) and its range-weighted generalization. The RWHT is very robust, allowing some 15 people to move around in the room during the experiments. The HT as such was used on images in [13] for finding corners and floor-wall intersections. It turns out that the HT is more efficient on range data than on images.

One problem all these systems have in common is the extensive and time-variable computing required by complex navigation algorithms. In this paper the time delay during computation is modelled and included in the algorithms. In effect, the dead reckoning and the observation parts of the Kalman filter are partially separated.

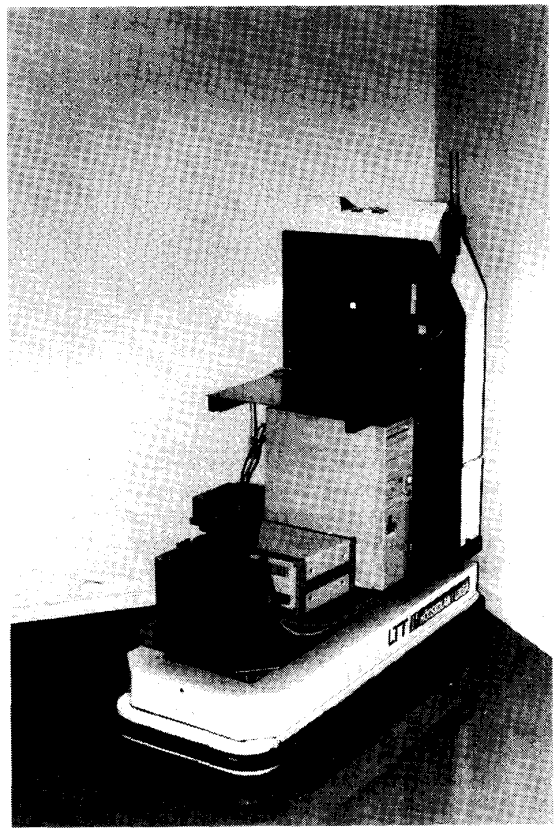

*Figure 1. The mobile robot used in the experiments. The scanning range-measuring laser is mounted on the front. The robot has three wheels, with odometers on the two rear wheels, and steering and traction on the front wheel. The maximal speed of the robot is 0.8 m/s and the maximum steering angle is 90 degrees. The range-measuring laser system is controlled using a T800 transputer. The Hough transform is computed on an i486-based PC standing just in front of the tower of the robot. The computer for motion control of the robot is MC68020-based.*

## EXTRACTING OBSERVATIONS FROM THE LASER MEASUREMENTS

This section illustrates how the Hough transform extracts flat surface elements (walls) from the range measurements of the scanning laser and how the door opening is detected. The measurements are presented as a polar curve and not as a traditional image. The Hough transform of a range scan is 'cleaner' and much more reliable than the Hough transform of a typical image. Thanks to occlusion in the range scan parallel lines are unlikely to occur close to each other. Hence the lines are well separated in the Hough space. A typical range scan is shown in Fig. 2.

The walls are modelled by the perpendicular distance $d$

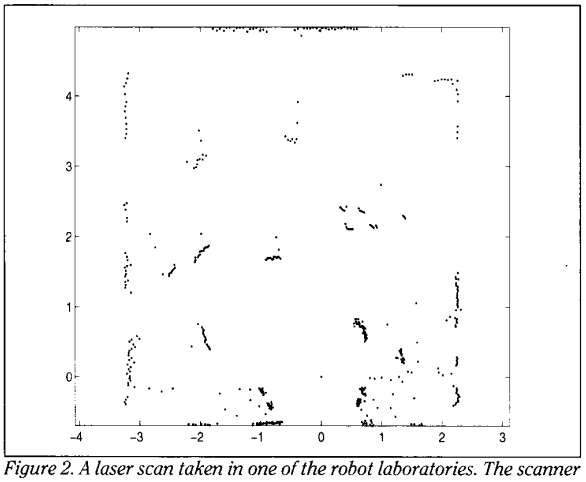

*Figure 2. A laser scan taken in one of the robot laboratories. The scanner is at position 0,0. The scanning range-measuring laser used is an IBEO Ladar-2D. The laser beam is about 4 cm in diameter and the maximum range is 32 m. The standard deviation in range is approximately 2 cm. A sector of 270 degrees is sampled with an angular resolution of 0.6 degrees. The mirror rotates continuously with 8 rotations per second giving 450 readings for each rotation.*

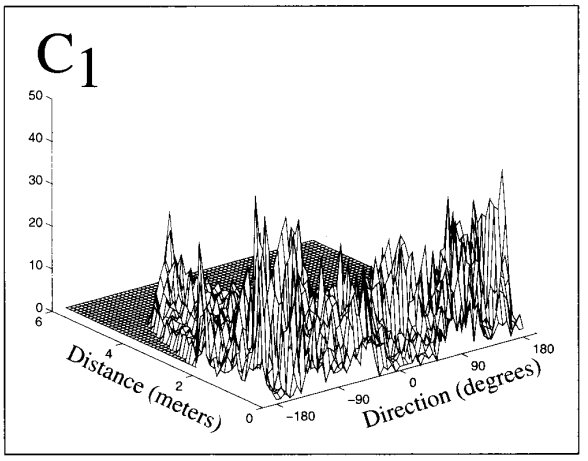


*Figure 3. The Hough transform $C_1(\gamma, d)$ of the room in Fig. 2. The walls can be extracted as peaks in the Hough transform. The noise from small objects near the laser makes it hard to detect the walls. The vertical scale is the histogram count. For both Fig. 3 and 4 the resolution is 6 degrees and 10 cm.*

from the robot, and the angle $\gamma$ to the perpendicular relative to the robot's orientation. The range scan is a set of points in polar coordinates $\{r_i, \varphi_i\}$ relative to the robot. The range scan is taken while the robot moves and is thus somewhat distorted by the motion. It is simple to correct the distortion caused by the motion by assuming a constant velocity during the 0.1 seconds required for one 270 degree scan. This is, however, not done below since at 0.5 m/s the distortion is small.

## The Hough Transform

To find the walls relative to the robot a weighted version of the Hough transform is used. The $g$-weighted Hough transform $C(d, \gamma)$ is defined as

$$C(d, \gamma) = \sum_i w(r_i \cos(\varphi_i - \gamma) - d) g(r_i, \varphi_i, \gamma) \quad (1)$$

where $w$ is a window function and $g$ is a weighting function to be selected below. The argument in $w$ is equal to the shortest distance between the point $(r_i, \varphi_i)$ and the line $(d, \gamma)$.

Currently a unit rectangular window function $w(x)$ of width $2a$ is used.

$$w(x) = \begin{cases} 1 & |x| \le a \\ 0 & |x| > a \end{cases} \quad (2)$$

This choice allows an efficient implementation. For the case $g \equiv 1$ it follows that

$$C_1(d, \gamma) = \textit{the number of measurements inside the strip with width } 2a \textit{ centered around the line } (d, \gamma) \quad (3)$$

After discretization in $(d, \gamma)$, the special transform $C_1$ is thus a counting function making $C_1(d, \gamma)$ a *histogram*. The transform $C_1$ of the scan in Fig. 2 is plotted in Fig. 3.

In the range scan the sampling is uniform with angular steps $\delta_\varphi$. As the distances increase, each sample corresponds to a longer surface segment. To compensate for this the surface sampling rate is introduced as the weighting function $g_2$, giving

$$C_2(d, \gamma) = \sum_i w(r_i \cos(\varphi_i - \gamma) - d) \left| \frac{r_i}{\cos(\varphi_i - \gamma)} \right| \quad (4)$$

The weighting makes $C_2$ *sensitive* to even single spurious measurements at large distances – especially the cosine term. A compromise is to use only range weighting, $g_3 = r_i$, giving

$$C_3(d, \gamma) = \sum_i w(r_i \cos(\varphi_i - \gamma) - d) r_i \quad (5)$$

called the range-weighted Hough transform. This could still be sensitive to spurious measurements at large distances. However, the limited range (30 meters) of the laser limits this effect. Without such a range limit some other kind of validity check of the measurements might be necessary. For the room in Fig. 2 range-weighted Hough transform is plotted in Fig. 4. At short ranges the signal-to-noise ratio has increased. More plots of the HT and RWHT of range measurements are given in [8] for indoor scenes and in [18] for an outdoor scene with a building.

The peaks in the RWHT are found by first searching for the single highest peak. The measurements associated with this peak are then removed from the Hough transform and the procedure is repeated until all major peaks have been found.

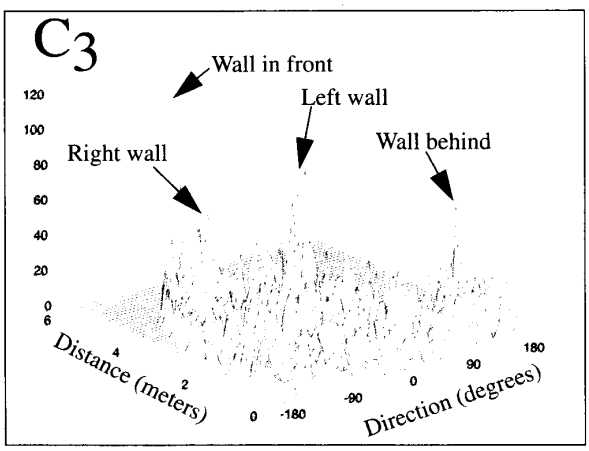


*Figure 4. The range weighted Hough transform $C_3(\gamma, d)$ of the room in Fig. 2. The four walls give clear peaks while the small objects close to the laser are suppressed by the range weighting. The vertical scale is the weighted histogram count, roughly proportional to the visible length of the walls.*

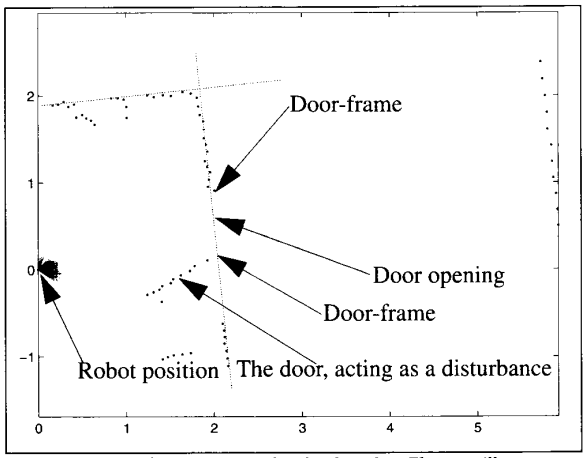


*Figure 5. Part of a rangescan taken by the robot. The scan illustrates how the doorway is found where measurements are detected beyond the wall. The scale is in meters with the robot located at (0, 0). Only every third measurement is plotted.*

**Each peak in the histogram gives an estimate of the perpendicular distance and the relative orientation of a surface. The Hough peak is then enhanced using a robust least squares method giving the observation $(\hat{d},\hat{\gamma})$.**

When searching for the walls of a rectangular room, the reliability of the estimate can be increased by searching for groups of four peaks at 90 degree intervals, rather than for single peaks. Increased scores are thus given to walls that are orthogonal or parallel to other walls. This method is used in the experiments described in the experimental results section. This has the additional advantage that we need to find only one such group of four peaks, thus making the iterative approach for finding several peaks unnecessary.

In the navigation experiments the angular resolution of the Hough transform was usually about three degrees (120 angular steps for a normal Hough transform or 30 for the room-extracting version). The distance resolution was usually 2.5 cm. The required computation time is proportional to the product of the number of angular steps and the number of measurements. It is not affected significantly by the distance resolution.

### Extracting the Position of a Door

Doorways are detected by searching for several consecutive measurements *beyond* the wall, see Fig. 5. If the detected opening has the correct size, then it is classified as an observation of a door opening. The position of the opening is estimated as the mean of the positions of the two door-frames. The beam width and the angular step $\delta_\varphi$ give approximately the sum of two uniformly distributed noise sources and are approximated by Gaussian noise.

## NAVIGATION IN A CLUTTERED ROOM AND THROUGH AN OPEN DOOR

This section describes how the position of the mobile robot inside a cluttered rectangular room can be estimated while the robot is moving, and how the robot can navigate through an open door.

### Observations and the State Vector

The observations of the walls are extracted by the Hough transform and described by the perpendicular distance $d$ and direction $\gamma$ relative to the robot's pose. This can be used to model any polygonal building. For the special case of a room with four walls the model relative to the robot will be

$$\left[d_1\ \gamma_1\ d_2\ \gamma_2\ d_3\ \gamma_3\ d_4\ \gamma_4\right] \tag{6}$$

If the room is rectangular, then the walls will be at 90 degree intervals and only one angle $\gamma$ is needed to describe the orientation of the room relative to the robot, see Fig. 6. Appending the position $d_d$ of the door gives the observation vector at time $t_k$ as extracted by the Hough transform and a subsequent least squares tuning.

$$Z(t_k) = \left[\hat{d}_1(t_k)\ \hat{d}_2(t_k)\ -\hat{\gamma}(t_k)\ \hat{d}_3(t_k)\ \hat{d}_4(t_k)\ \hat{d}_d(t_k)\right] \tag{7}$$

For the state vector a coordinate system has been placed in one of the corners of the room giving $x = d_1$, $y = d_2$ and $\theta = -\gamma$. The constant (but uncertain) size of the room is used to replace the two remaining distances, $x_s = d_1 + d_3$ and $y_s = d_2 + d_4$. This makes the time-varying pose of the robot and the constant size of the room explicit. For clarity of presentation we assume that the door is on a wall parallel with the y-axis, giving the state vector:

$$X(t_k) = \left[x(t_k)\ y(t_k)\ \theta(t_k)\ x_s\ y_s\ y_d\right]^T \tag{8}$$

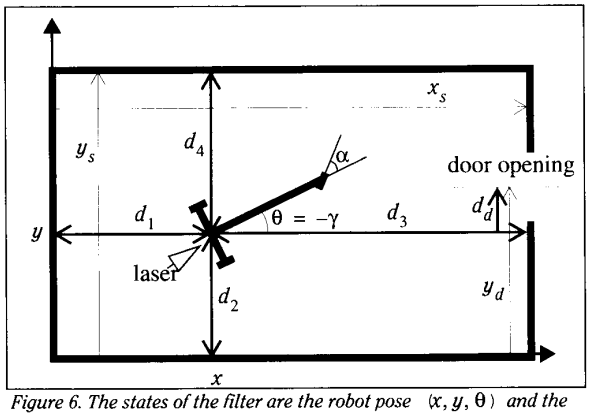


*Figure 6. The states of the filter are the robot pose $(x, y, \theta)$ and the size of the room $(x_s, y_s)$. The observations extracted by the Hough transform are $(d_1, d_2, d_3, d_4, \gamma)$. To navigate through a door $y_d$ is also needed. $\alpha$ is the angle of the steering wheel.*

*To summarize*: the first three components in the state vector $X(t_k)$ are the pose of the robot. One of the corners in the room is used to define the global reference frame. The last three components are the size $x_s$, $y_s$ of the room and the position $y_d$ of the open door. These three state variables can be viewed as the "map" of the room.

If the laser is located at $(0, 0)$ on the robot we get the *linear* observation model

$$Z(t_k) = HX(t_k) + w(t_k) \quad \text{where } H = \begin{bmatrix} 1 & 0 & 0 & 0 & 0 & 0 \\ 0 & 1 & 0 & 0 & 0 & 0 \\ 0 & 0 & 1 & 0 & 0 & 0 \\ -1 & 0 & 0 & 1 & 0 & 0 \\ 0 & -1 & 0 & 0 & 1 & 0 \\ 0 & -1 & 0 & 0 & 0 & 1 \end{bmatrix} \tag{9}$$

During the experiments the laser was not mounted at $(0, 0)$. Eq. (9) gives the principle but the actual observation function used in the system is nonlinear.

A simpler system can be designed using only the position of the door relative to the robot (three parameters). The disadvantage of a simpler system is that the observation of the door is rather inaccurate compared to the observation of the room. By filtering several observations we can obtain a very good estimate of the door's position relative to the walls of the room. By measuring the robot position relative to the walls during motion we can maintain a good estimate of the robot position relative to the room, and indirectly the door. This allows the robot to pass through a door with 1 cm fluctuations even though the observation of the door position has at least a 2 cm uncertainty.

## Dead Reckoning

The robot's pose can be expressed in different frames. For $t > t_k$ the displacement of the robot since time $t_k$ is written as

$${}^kP(t) = \left[{}^kx(t) \; {}^ky(t) \; {}^k\theta(t)\right]^T \tag{10}$$

where $\{k\}$ is a frame defined by the pose of the robot at time $t_k$ - see Fig. 7. The superscript $k$ denotes that the pose is expressed in the coordinate system of frame $\{k\}$. The pose expressed in the global reference is written as $P(t) = \left[x(t) \; y(t) \; \theta(t)\right]^T$.

The pose of the robot at time $t$ in the global reference frame can be expressed using the robot's pose $P(t_k)$ at time $t_k$ and the displacement ${}^kP(t)$.

$$P(t) = P(t_k) + R(\theta(t_k)) \; {}^kP(t) \tag{11}$$

$$\text{where } R(\theta) = \begin{bmatrix} \cos\theta & -\sin\theta & 0 \\ \sin\theta & \cos\theta & 0 \\ 0 & 0 & 1 \end{bmatrix} \tag{12}$$

Also, (11) recursively updates the dead reckoning estimate of the pose $P(t_k)$ of the robot. The estimation error $\tilde{P}(t) = P(t) - \hat{P}(t)$ propagates as

$$\tilde{P}(t_{k+1}) = \tilde{P}(t_k) + \left[R(\hat{\theta}(t_k)) - R(\theta(t_k))\right] \; {}^k\hat{P}(t_{k+1}) + R(\theta(t_k)) \; {}^k\tilde{P}(t_{k+1}) \tag{13}$$

where ${}^k\tilde{P}(t_{k+1})$ is the dead reckoning error between $t_k$ and $t_{k+1}$. The error ${}^k\tilde{P}(t_{k+1})$ is modelled as zero-mean Gaussian with covariance matrix ${}^kQ(t_{k+1})$. A linear approximation of (13) valid for small errors $\tilde{\theta}$ is

$$\tilde{P}(t_{k+1}) \approx F_k\tilde{P}(t_k) + R(\hat{\theta}(t_k)) \; {}^k\tilde{P}(t_{k+1}) \tag{14}$$

where

$$F_k = \begin{bmatrix} 1 & 0 & -{}^k\hat{x}(t_{k+1})\sin\hat{\theta}(t_k) - {}^k\hat{y}(t_{k+1})\cos\hat{\theta}(t_k) \\ 0 & 1 & {}^k\hat{x}(t_{k+1})\cos\hat{\theta}(t_k) - {}^k\hat{y}(t_{k+1})\sin\hat{\theta}(t_k) \\ 0 & 0 & 1 \end{bmatrix} \tag{15}$$

The approximation is used for updating the covariance matrix.

To avoid large linearization and modelling errors the odometer estimate is updated with a higher frequency (50 Hz) than the Kalman filter ($\approx 1$ Hz). The higher frequency is also needed to supply the control law with up-to-date position estimates.

Between the two range scans at time $t_k$ and $t_{k+1}$ the estimate of ${}^kP(t)$ and the covariance matrix ${}^kQ(t)$ are updated at $(t_{k,1}, t_{k,2}, \ldots, t_{k+1})$. The displacement ${}^{k,l}P(t_{k,l+1})$ of the ro-

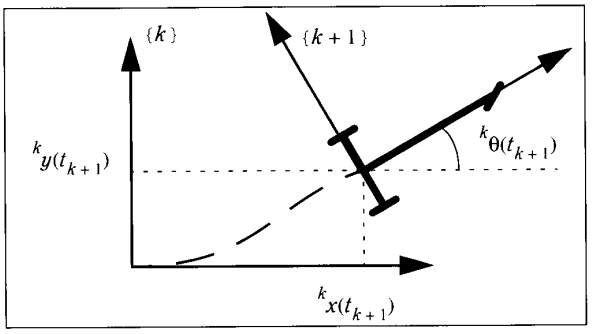


*Figure 7. Pose of the robot given in frame $\{k\}$ defined by the robot at time $t_k$. The trajectory between $t_k$ and $t_{k+1}$ is modelled as a sequence of circular arcs.*

bot between time $t_{k,l}$ and $t_{k,l+1}$ is computed from the odometer readings. The uncertainties in the odometer readings are modelled by a covariance matrix $^{k,l}Q(t_{k,l+1})$. $^{k}P(t_{k,l+1})$ and $^{k}Q(t_{k,l+1})$ are computed using (11) and (14) modified such that the updated pose is expressed in the local frame $\{k\}$.

### Navigation

The navigation system is summarized in Table 2. There are two processes active. The dead reckoning process is sampling at high frequency while the localization process operates in the background.

When, at time $t_k$, a measurement scan is taken, the background process first extracts the observations from the measurements and then uses these observations $\hat{Z}(t_k)$ to filter the estimate $\hat{X}(t_k|t_{k-1})$, predicted at time $t_k$, using an extended Kalman filter, [1]. The result is the filtered estimate $\hat{X}(t_k|t_k)$. The time is now $t_{k+1}$ and the displacement $^{k}\hat{P}(t_{k+1})$ of the robot since $t_k$ has been computed by the dead reckoning process. This is used with (5) to compute the new prediction $\hat{X}(t_{k+1}|t_k)$ and the associated covariance matrix $\Sigma(t_{k+1}|t_k)$.

$$\hat{X}(t_{k+1}|t_k) = \hat{X}(t_k|t_k) + \begin{bmatrix} R(\hat{\theta}(t_k|t_k)) \\ 0 \end{bmatrix} {}^{k}\hat{P}(t_{k+1})$$

$$\Sigma(t_{k+1}|t_k) = \begin{bmatrix} F_k & 0 \\ 0 & I \end{bmatrix} \Sigma(t_k|t_k) \begin{bmatrix} F_k^T & 0 \\ 0 & I \end{bmatrix} + \quad . \quad (16)$$

$$+ \begin{bmatrix} R(\hat{\theta}(t_k|t_k)) \\ 0 \end{bmatrix} {}^{k}Q(t_{k+1}) \begin{bmatrix} R(\hat{\theta}(t_k|t_k)) \\ 0 \end{bmatrix}^T$$

Note that $\hat{X}(t_k|t_k)$ is not available until $t_{k+1}$ due to the computational delay in the extraction. An estimate $\hat{X}(\,)$ is available to the control law whenever requested

**Table 2 The Dead Reckoning and the Localization are Computed in Parallel as Two Separate Processes.**

| Time | Dead Reckoning Process | Localization Process |
|---|---|---|
| $t_k = t_{k,0}$ | $^{k}\hat{P}(t_{k,0}) = 0$<br>$^{k}Q(t_{k,0}) = 0$ | $\{r, \gamma\}$ measured with laser. |
| $t_{k,1}$ to $t_{k,L_k}$ | The displacement $^{k}\hat{P}(t_{k,l})$ and the covariance matrix $^{k}Q(t_{k,l})$ are recursively updated using odometer readings. | Extract the vector $Z(t_k)$ from the range scan. Use the EKF to compute $\hat{X}(t_k|t_k)$ and $\Sigma(t_k|t_k)$. |
| $t_{k+1}$ | The displacement $^{k}\hat{P}(t_{k+1})$ and the covariance matrix $^{k}Q(t_{k+1})$ are updated as above and stored. | $\hat{X}(t_{k+1}|t_k)$ and $\Sigma(t_{k+1}|t_k)$ are computed according to eq. (8). |

$$\hat{X}(t) = \hat{X}(t_k|t_{k-1}) + \begin{bmatrix} R(\hat{\theta}(t_k|t_{k-1})) \\ 0 \end{bmatrix} {}^{k}\hat{P}(t) \qquad t \geq t_k \quad (17)$$

### The Control Law

The position estimator introduced above makes a large variety of navigation tasks possible. Each of them require a good control law. The two most basic navigation tasks are positioning and trajectory following. Several control laws have been studied (e.g. [12], [17] and [20]) and can be used in this navigation system. The control law used to evaluate the navigation in this paper is a control law for following straight lines adapted to the task of passing through an open door.

The control signal is the angle $\alpha$ of the steering wheel and the desired trajectory is a straight line parallel with the x-axis at $y = y_d$, see Fig. 6. The chosen control law is given as

$$\alpha(t) = -\arctan\left(k_1 (y(t) - y_d(t)) + k_2 \sin\theta(t)\right) - \theta(t) \quad (18)$$

By choosing the feedback constants $k_1$ and $k_2$ the amount of overshoot can be controlled. Note that the front wheel has to overshoot to properly align the rear wheels. Compare with Fig. 9. A preliminary gain scheduling was used for $k_1, k_2$.

## EXPERIMENTAL RESULTS

The algorithms have been tested with the robot described in Fig. 1. A range scan taken by the laser is shown in Fig. 2. This section presents a number of experimental results and a discussion of error sources. The most serious errors are caused by erroneous interpretation of the range data.

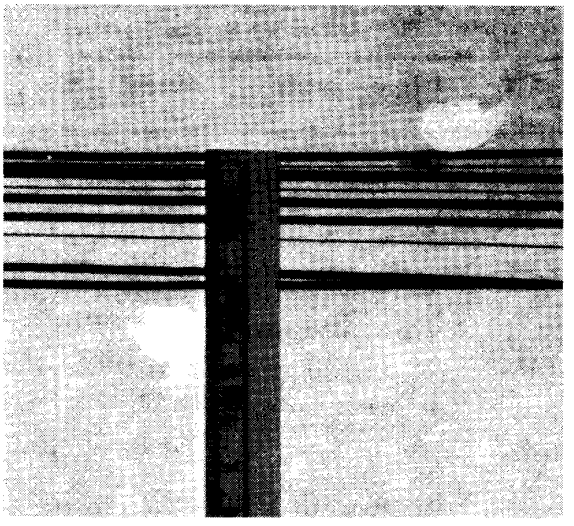

*Figure 8. The photograph shows the trajectories plotted on the floor just in front of the door. A pen was mounted under the robot. The large initial maneuvers are completed, and the trajectories are now almost parallel. The visible part of the measuring rod is about 10 cm. Plots similar to this, but with a finer pen, were used to evaluate the repeatability presented in Table 3.*

### Navigation in a Corridor

The first tests of the algorithms were made in a long corridor. When navigating in a corridor there will be two distinct peaks in the Hough transform. The feedback law is designed such that the peaks are at equal distance and perpendicular to the heading of the robot. Thus the robot will move along the middle of the corridor.

At the full speed, 0.8 m/s, of the robot the repeatability of the motion is better than ±1 cm. Moreover, the laser was disturbed intentionally by flapping a paper close to the it without noticeable effect on the navigation.

### Navigation through an Open Door

The robot autonomously finds the walls and doors of the room and, for passage, selects one door. It is capable of adapting to new situations, and will stop and search for a new door if the door it is heading for is closed during the approach.

Although the laser can measure eight full scans every second, the present computer is only capable of processing one scan per second. During a passage through the door at 0.5 m/s only about six to ten scans are used before the passage.

A pen is mounted under the robot fairly close to the midpoint between the front and rear wheels. Fig. 8 is a photo of eight trajectories plotted on the floor with this pen. In this case the speed was 0.2 m/s. The fluctuations of the plotted trajectories converges within 1 cm just before the robot passes through the door. Table 3 gives the result of a statistical analysis for this type of 'ground truth.' The plotted lines were evaluated using a measuring rod. The results will be compared and discussed below.

During the tests, extracted wall coordinates, estimates of the state, etc. were recorded. The trajectories plotted in Fig. 9

**Table 3 Standard Deviations Showing the Repeatability during Tests at Two Speeds and with Different Starting Positions.**

| | 0.2 m/s | 0.5 m/s |
|---|---|---|
| "Easy" runs, from starting positions about three meters in front of the door and within 20 degrees. | $\sigma_y \approx 0.5$cm<br>$\sigma_\theta \approx 5$mrad | $\sigma_y \approx 0.7$cm<br>$\sigma_\theta \approx 4$mrad |
| "Difficult" runs, from starting positions closer to, and to the side of, the door (see Fig. 9). | $\sigma_y \approx 0.9$cm<br>$\sigma_\theta \approx 10$mrad | $\sigma_y \approx 1.2$cm<br>$\sigma_\theta \approx 8$mrad |

are the Kalman filter estimates of the robot's position relative to the estimated position of the door. More precisely, the front wheel curves are

$$\begin{bmatrix} \hat{x}_{\mathrm{fw}}(t_k) & \hat{y}_{\mathrm{fw}}(t_k) - \hat{y}_{\mathrm{d}} \end{bmatrix} \tag{19}$$

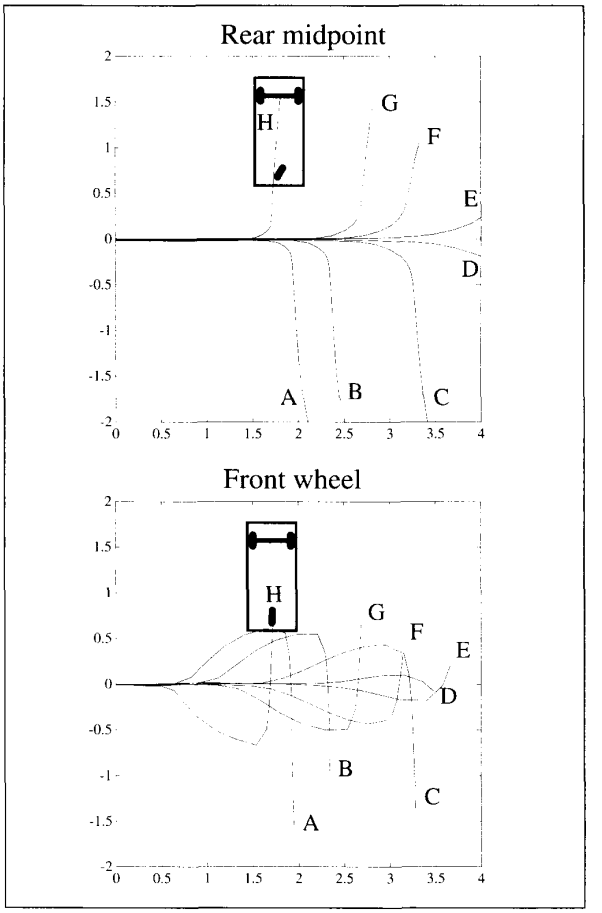


*Figure 9. Experimental trajectories when starting from several different starting positions. The lower plot is the front wheel and the upper is the rear midpoint. Note that the overshoot of the front wheel is necessary to align the robot with the perpendicular of the door. The plotted trajectories are the Kalman filter estimates of the robot's position relative to the door.*

where the estimates $\hat{x}_{fw}, \hat{y}_{fw}$ of the front wheel are computed from $\hat{x}, \hat{y}, \hat{\theta}$ in the Kalman filter.

The curves in Fig. 9 show the transients. Although not plotted here, a zoom-in on the last 50 cm shows fluctuations very similar to the plots on the floor.

Two elements in the state vector are the size of the room. A number of estimates are plotted in Fig. 10. Each point is from a complete scan obtained by a least squares fit initiated by the four peaks of the Hough transform. There are three categories of errors. Noisy measurements occur, giving a standard deviation of 0.3-1.2 cm depending, among other factors, on how long a segment of the wall is observed. A calibration error arises, giving a constant offset. The differences between A and H are interpreted as disturbance by the heating radiators on the wall. This type of disturbance is a typical association error and, if large, is the most serious as it cannot be compensated by either calibration or simple statistical methods.

### Erroneous Association and Conventional Error Sources

During navigation one side of a corridor was actually a several meters long glass wall. The frames of the glass panes gave a weak peak in the Hough transform, while the wall of the room behind the glass panes gave the strongest peak. This is a typical source of erroneous associations. It can be 'resolved' by sensor fusion (relative to the model classes in [18]) or by using a detailed map.

*Absolute errors:* The position of the laser on the robot, an asymmetric laser beam and angular offset in the scanner give systematic errors in the measured range. Most of these errors can be reduced by *calibration*.

*Dynamic errors:* Timing uncertainties, such as exactly when the scan was taken, is a genuine noise source for the dynamic behavior.

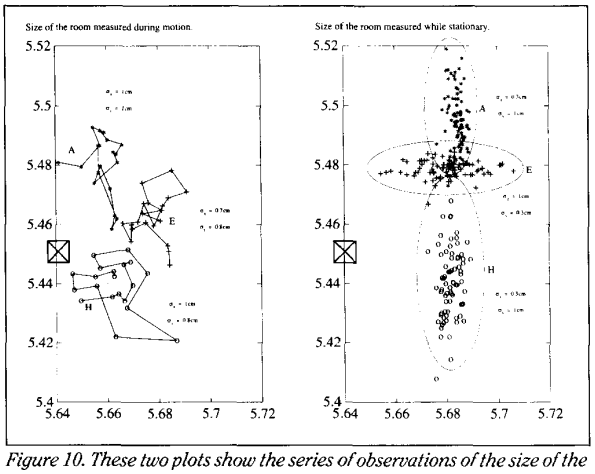


*Figure 10. These two plots show the series of observations of the size of the room. Each point in the plot indicates the size given by one observation. The true size of the room is 5.45 by 5.64 meters. (Left) The plot shows how the measured size of the room varies as the robot moves. The 'A,' 'E' and 'H' plots are taken from trajectory 'A,' 'E' and 'H' in Fig. 9 respectively. (Right) The distribution of size measurements when the robot is stationary is shown with the robot at three different poses, the starting point of trajectory 'A,' 'E' and 'H' respectively. The ⊠ symbol marks the actual size of the room. The differences between measurements taken at different angles and positions are probably due to association errors between the wall and the heating radiators mounted on it.*

*Geometric errors and clutter:* Many small objects like the 28 legs of the Board of Graduate Research have little effect on the Hough transform and do not disturb the navigation of the robot. Two heating radiators 4 cm from one wall, which covered 40% of the length of the wall, were more disturbing. It is hard to model the consequences on the trajectory caused by these types of correlated range noise.

*Geometrical ambiguities:* When entering a new room of unknown size there might be some initial ambiguities. A large rectangular object like a table might be interpreted as a wall and give rise to a 'large false door.' The robot will automatically correct itself when it finds the true wall behind the 'large false door.' Also, non-parallel walls in a rectangular room might cause the association gates to fail. If the room is irregular the ambiguities when choosing the four walls have to be dealt with by both refining the models, and by trading performance for robustness.

## CONCLUSIONS, GENERALIZATIONS AND FUTURE WORK

The problem studied was navigation in cluttered rooms using a range-measuring laser as the geometrical sensor and the Hough transform to extract geometrical information.

A *robust* algorithm was developed for simultaneous estimation of the robot's pose in the room and the size of the room. Feedback laws were developed and *tested* for two cases, passage through an open door and navigation in corridors. The fluctuations in the experimental trajectories were smaller than ±1 cm and ±0.6 degrees at 0.5 m/s for passage through a door. A corridor gave ±1 cm at 0.8 m/s.

A detailed noise budget is complicated, since there are several non-negligible dependencies among the variables. The *preliminary conclusion* is that, without any special compensations, it is possible to navigate within ±1-2 cm and with variations of ±1 cm. Sharp turns at maximum speed (0.8 m/s) will give larger errors.

Most types of standard noise (electronic, dynamic, jitter, etc.) give a fairly predictable behavior of the robot. Also an analysis seems fairly straightforward using tools from automatic control and signal processing. However, the most serious disturbances are erroneous geometrical interpretations giving association errors. This is an important topic for forthcoming studies, i.e methods and algorithms for combining multiple sensors, geometrical rules and maps without running into combinatorial explosions.

The model, algorithm and tests described above were restricted to one rectangular room. This introductory test can be *generalized* for an 'entire building having a polygonal architecture.' For each visible wall in the building it is possible to extract the coordinates $(d, \gamma)$ with the Hough transform. The last three components in the state vector (8) are replaced with the coordinates of all the observed walls, compare with (6). The observation vector in (7) is replaced with the coordinates of all the walls that are extracted at time $t_k$. This implies that the estimate of the state vector will be augmented with new states as new walls are observed by the moving robot. This generalized map-building and navigation system has recently been implemented on two new mobile robots, one of which is described in [14]. Expanding the model from one room to two rooms and finally to an entire building introduces new problems in that matching observations to landmarks becomes gradually more difficult and time-consuming.

## REFERENCES


[1] B. D. O. Anderson, J. B. Moore, *Optimal Filtering*. Prentice Hall, 1979.

[2] S. Atiya, G. D. Hager, "Real-Time Vision-Based Robot Localization," *IEEE Trans. on Robotics and Automation*, Dec. 1993.

[3] N. Ayache, O. D. Faugeras, "Maintaining Representations of the Environment of a Mobile Robot," reprinted in *Autonomous Robot Vehicles*. Springer Verlag, 1990.

[4] J. Crowley, "World Modelling and Position Estimation for a Mobile Robot Using Ultrasonic Ranging," *IEEE Conf. Robotics and Automation*, 1989, pp 674-680.

[5] I. J. Cox, "Blanche - An Experiment in Guidance and Navigation of an Autonomous Mobile Robot," *IEEE Trans. on Robotics and Automation*, Apr. 1991.

[6] I.J. Cox, G. T. Wilfong, Eds, *Autonomous Robot Vehicles*. Springer Verlag, 1990.

[7] A. Elfes, "Sonar-Based Real-World Mapping and Navigation," *Autonomous Robot Vehicles*. Springer Verlag, 1990.

[8] J. Forsberg, U. Larsson, P. Åhman, Å. Wernersson, "The Hough Transform Inside the Feedback Loop of a Mobile Robot," in *Proc. IEEE Conf. Robotics and Automation* (Atlanta, USA), May 1993, pp 791-8.

[9] G. Foux, M. Heymann, A. Bruckstein, "Two-Dimensional Robot Navigation among Unknown Stationary Polygonal Obstacles," *IEEE Trans. on Robotics and Automation*, Feb. 1993.

[10] J. Hallam, *Intelligent Automatic Interpretation of Active Marine Sonar*. PhD thesis, University of Edinburgh, 1984.

[11] K. Hyyppä, "Luleå Turbo Turtle (LTT)," *Proc. IROS*, 1989, pp. 620-623.

[12] Y. Kanayama et. al., "A Stable Tracking Control Method for an Autonomous Mobile Robot," *IEEE Int. Conf. on Robotics and Automation*, 1990.

[13] A. Kosaka, A. Kak, "Fast Vision-Guided Mobile Robot Navigation Using Model-Based Reasoning and Prediction of Uncertainties," *Image Understanding*, Nov. 1992.

[14] U. Larsson, J. Forsberg, Å. Wernersson, "On Robot Navigation Using Identical Landmarks: Integrating Measurement from a Time-of-Flight Laser," *IEEE Int. Conf. on Multisensor Fusion and Integration for Intelligent Systems*, 1994.

[15] J. Leonard, H. Durrant-Whyte, *Directed Sonar Sensing for Mobile Robot Navigation*, Kluwer Academic Publishers, 1992.

[16] J. Leonard, H. Durrant-Whyte, I. J. Cox, "Dynamic Map Building for an Autonomous Mobile Robot," *IROS-90*, pp 89-95

[17] Z. Li, J. F. Canny, *Nonholonomic Motion Planning*, Kluwer Academic Publishers, 1993.

[18] P. Klöör, Å. Wernersson, "On Motion Estimation for a Mobile Robot Navigating in Natural Environment," in *Proc. IROS*, 1992, pp 1421-28.

[19] P. Moutarlier, R. Chatila, "Stochastic Multisensory Data Fusion for Mobile Robot Location and Environment Modelling," *Robotics Research 5th Int. Symp.* pp 85-94

[20] C. Samson, K. Ait-Abderrahim, "Feedback Control of a Nonholonomic Wheeled Cart in Cartesian Space," *IEEE Int. Conf. on Robotics and Automation*, 1991.

[21] R. Urick, *Principles of Underwater Sound*. McGraw-Hill, 1983.

[22] Å. Wernersson, U. Wiklund, U. Andersson, K. Hyyppä, *"Vehicle Navigation Using 'Image Information': on Association Errors,"* *IAS-2*, pp 814-822, 1989.


## ABOUT THE AUTHORS

Johan Forsberg received the M.S. degree in electrical engineering from Luleå University of Technology in 1992. He is currently pursuing the Ph.D. degree in Robotics at Luleå University of Technology. His research interests are in the area of sensing and navigation for mobile robots. He is a member of the Board of Graduate Studies and Research at Luleå University of Technology.

Ulf Larsson received the M.S. degree in electrical engineering from Luleå University of Technology in 1992. He is currently pursuing the Ph.D. degree in Robotics at Luleå University of Technology. His research interests are in the area of sensing and navigation for mobile robots.

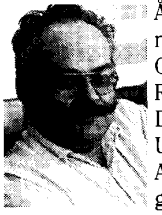

Åke Wernersson received an M.S. in Engineering Physics from Chalmers and Ph.D. in Optimization and System Theory from the Royal Institute of Technology, Stockholm. Docent in Automatic Control at Linköping University, and now professor in Robotics and Automation at Luleå University of Technology. Three years with SAAB Avionics and eight years with FOA (Radar Systems and Information Technology).

His current research is on models and algorithms for extracting geometric shapes, features and motion using non-contact sensors (laser, range camera, coherent ultrasonic). Typical applications are sensor feedback for robot assembly, curve and surface following, vehicle navigation and telerobotics.